Analysis of turbulence models fitted to site, and their impact on the response of a bottom-fixed wind turbine

Analysis of turbulence models fitted to site, and their impact on the response of a bottom-fixed wind turbine

A Nybø[1], FG Nielsen[1] and M Godvik[1,2]

[1] Geophysical Institute, and Bergen Offshore Wind Centre, University of Bergen, Norway
[2] Equinor, Bergen, Norway

E-mail: astrid.nybo@uib.no

Abstract. This study compares a wind field recommended by the wind turbine design standards to more realistic wind fields based on measurements. The widely used Mann spectral tensor model with inputs recommended by the standard, is compared to FitMann, the Mann model with inputs fitted to measurements and TIMESR; using measured time series combined with the Davenport coherence model. The Mann model produces too low energy levels at the lowest frequencies of the wind spectra, while the wind spectra generated by FitMann approaches the measured values. TIMESR reproduces the measured spectral values at all frequencies. The different models give similar vertical coherence, while the Mann and FitMann models give lower horizontal coherence than TIMESR. Investigating the wind loads on a bottom-fixed 10-MW wind turbine, the spectra for the tower bottom fore-aft and blade root flapwise bending moment follow the shape of the wind spectra closely at low frequencies. The low-frequency range is important for the blade root and in particular the tower bottom bending moment. Thus, the TIMESR model, followed by FitMann, is assumed to give the most accurate fatigue estimates. For the specific situation analysed in this study, the FitMann model gives only 18 and 5 % lower estimates than TIMESR of the tower bottom and blade root damage equivalent bending moments, while the Mann model gives 27 % and 12 % lower estimates. The tower top yaw and fore-aft bending moments depend on the wind coherence. For the specific situation analysed in this study, the FitMann model gives 9 and 5 % higher estimates of the tower top yaw and tower top damage equivalent (bending) moments compared to TIMESR, while the Mann model gives 23 % and 18 % higher estimates. Since only measurements of the vertical coherence are available, it is not clear which model is superior for the tower top moments. However, the importance of a proper coherence model is documented.

1. Introduction

In the design of wind turbines, turbulence models are used to simulate wind fields for load estimation. The International Electrotechnical Commission (IEC) wind turbine design standards [1–3] recommend e.g. the Mann spectral tensor model [4] for this purpose. The IEC standards further recommend a set of input parameters to this model, where only the turbulence intensity and wind profile are fit to actual site conditions.

The trends in the wind industry point towards larger rotor sizes and an increasing interest for offshore locations. These trends are partly connected, as the largest wind turbines are placed offshore due to easier blade transportation. Offshore, weather conditions are harsher and the total structural loads higher. With larger rotors, a larger variation in wind characteristics over

Table 1. Summary of wind field characteristics of the chosen situation.

Hub mean wind speed	12.4 m/s
Hub turbulence intensity	6 %
Power law exponent	0.06
Stability	Neutral

the swept area is expected. Therefore, a correct representation of turbulent wind becomes more important. In this context, the standard Mann model is challenged.

Fitting the input parameters of the Mann model to actual site conditions may serve as an alternative to easily adapt an existing well known model to various conditions, without adding time, cost and complexity excessively. This has been performed in academia to a large extent (e.g. by Mann [5], Sathe et al. [6], de Maré and Mann [7], Cheynet et al. [8, 9], Peña et al. [10, 11] and Chougule et al. [12–14]). Chougule et al. [13, 14] developed the Mann model further to account for buoyancy effects, requiring additional input parameter(s). The wind industry also challenges the widely used turbulence models recommended by the standard, as they are made for small turbines and for flow over flat terrain in neutral atmospheric conditions [15]. Fitting of the Mann parameters gives opportunities for evaluating the design of wind turbines in e.g. various atmospheric stability conditions. Even within neutral stability conditions, fitting of Mann to measurements may alter the corresponding response as compared to using the input parameters recommended by the IEC standard.

In this study, a fitting of the input parameters of the Mann model to neutral offshore conditions is performed, and the corresponding response of an offshore wind turbine is evaluated. This model, hereafter denoted FitMann, is compared to the Mann model with standard inputs, hereafter denoted Mann, and another easily available and fast turbulence model closely based on measurements, hereafter denoted TIMESR [16]. The latter model is originally based on Veer's model from 1988 [17], and uses time series and coherence parameters obtained from measurements as inputs. The turbulent structures of the wind fields generated by Mann, FitMann and TIMESR are evaluated in terms of the wind spectrum and coherence. The wind fields are used as inputs in a simulation tool for wind turbine design purposes, and the corresponding response is evaluated. The simulations are performed on a 10-MW bottom-fixed wind turbine. It is previously found [18] that the quasi-static response is important for the overall response, especially for the tower bottom and blade root flapwise bending moment. The response, in terms of response spectra and damage equivalent moments, is therefore evaluated with a special focus on frequencies below 0.1 Hz, hereafter denoted the low-frequency region. The mentioned literature covers fitting of the Mann model to various stability conditions over a range of different surfaces, but none of them compare the corresponding wind turbine response to the response obtained by using wind fields from other turbulence models.

2. Data and methods

2.1. Wind fields

Measurements from the offshore meteorological mast FINO1, located in the North Sea, are used as basis in this study. Sonic anemometers provide high-frequent measurements of the wind speed at several heights, which are processed according to Nybø et al. [19]. The TIMESR, Mann and FitMann models are used to create wind fields based on point measurements from three anemometers separated vertically in the range 40-80 meters above sea-level.

In the present study, only one specific wind condition is considered, see Table 1. The result from this specific case is thus not valid as life-time evaluation of the wind turbine, including

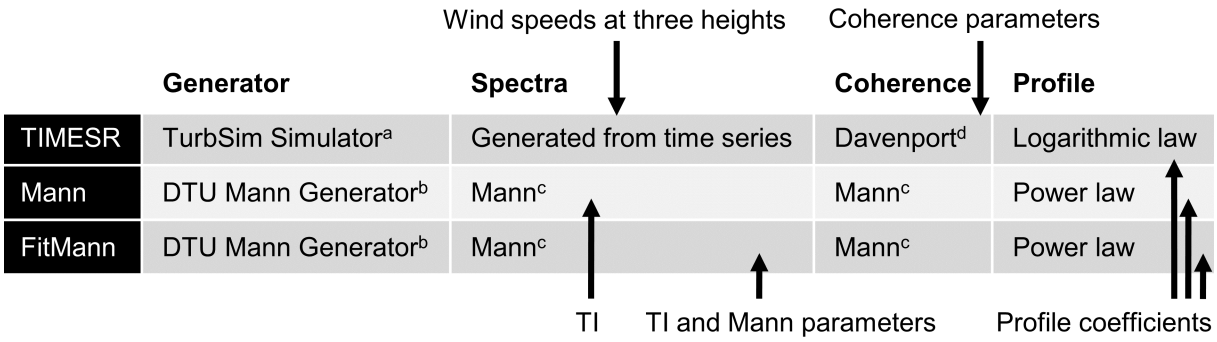

Figure 1. Scheme of wind field models, simulation software, spectra and coherence models and profile laws. Inputs from the FINO1 measurements are illustrated by the arrows. a from Jonkman [16], b from DTU Wind Energy [21], c from Mann [4] and d from Davenport [22].

Table 2. Input parameters to the DTU Mann Generator.

Model	$\alpha\epsilon^{2/3}(m^{3/4}s^{-2})$	$L(m)$	Γ
Mann	0.0229	33.6	3.9
FitMann	0.0168	73.6	3.8

all relevant wind speeds, atmospheric stability conditions etc. The chosen situation is almost stationary for one hour and has close to neutral stratification. The specific condition is thus well suited to be modelled by the numerical wind field models included in this study. The buoyancy term is not included in the Mann model as it is defined in the IEC standards and used by the offshore wind industry. It can therefore not simulate stable or unstable atmospheric conditions by definition. A mean wind speed just above rated wind speed is selected as this is considered crucial to the fatigue damage to the structure. The chosen situation has a typical turbulence intensity for the given wind speed at FINO1. The wind shear is rather low, even for offshore conditions. Türk et al. [20] found a power law coefficient of approximately 0.1 for the relevant wind speed at FINO1, and considerably lower for unstable atmospheric conditions. This indicates that the near-neutral atmospheric conditions of the chosen situation may be closer to unstable than stable.

The three wind fields are generated according to Figure 1. TIMESR uses time series from 40, 60 and 80 m above sea-level as input, creating spectra equal to the measured spectra at the input heights. The Davenport coherence model is applied in TIMESR, with parameters obtained from the coherence in the measurements. The profile coefficients (power law exponent of the power law and surface roughness of the logarithmic law) are found from the measured mean wind speeds at 40 and 80 m. The vertical mean velocity profiles obtained by the three models are very similar, even if different formulations of the vertical profile are used.

The turbulence characteristics of the wind fields generated by Mann are dependent on only three input parameters, namely the Kolmogorov constant multiplied with the rate of the viscous dissipation of specific turbulent kinetic energy to the two thirds, $\alpha\epsilon^{2/3}$, the length scale, L, and the non-dimensional parameter related to the lifetime of the eddies, Γ. IEC recommends L and Γ values according to the first row of Table 2 for wind turbines with hub heights higher than 60 m. $\Gamma = 0$ corresponds to isotropic turbulence and the von Kármán turbulence spectrum. Increasing $\alpha\epsilon^{2/3}$, moves the entire wind spectrum to higher energy levels, while increasing L and

Γ rather increases the energy level at low frequencies.

In Mann, as used in this study, the L and Γ given by the IEC wind turbine design standard are used. The standard recommends that $\alpha\epsilon^{2/3}$ is calculated according to Equation 1 [1, 4].

$$\alpha\epsilon^{2/3} = \frac{55}{18} * 0.4754 * \sigma_{iso}^2 l^{-2/3}. \quad (1)$$

The length scale parameter, l, is given by 0.8 times the turbulence scale parameter, Λ_1, which is 42 m for large wind turbines (hub height $\geq$ 60 m). The unsheared, isotropic variance, σ_{iso}, is according to the IEC standard given as 0.55 times the variance of the wind speed in the mean wind direction, σ_1. In the wind field generated by Mann in this study, σ_1 is calculated from the turbulence intensity, TI, and the wind speed, $\overline{u}_m$, of the measured time series, according to Equation 2.

$$\sigma_1 = TI * \overline{u}_m. \quad (2)$$

In FitMann, $\alpha\epsilon^{2/3}$, L and Γ are determined in order to fit the spectra generated by Mann to the spectra of the measured data at 80 m [23]. All Mann parameters are fitted simultaneously to the spectra of u, v, w and the real part of the cross spectrum of uw. A non-linear least-square fit is used. The spectrum and coherence still follow Mann formulations, thus the wind spectra of measurements are not reproduced as in TIMESR. The spectra of the time series at 80 m are estimated using Welch's algorithm [24] with a Hamming window, six segments, and 50 % overlapping. The spectra are bin averaged [25] before the fitting is performed. There is large uncertainty related to the very first frequency of the wind spectra, 0.0017 Hz, as it is only realized once within each block of the FFT. This frequency is still included in the fitting procedure, as it is important for response, and this study aims to achieve wind fields with similar characteristics and corresponding response as the measured time series.

The input parameters of Mann and FitMann are given in Table 2. The very large length scale obtained by FitMann moves the wind spectra to higher energy levels at low frequencies. This also indicates that the wind field is closer to a slightly unstable than a slightly stable situation. In order to conserve the total energy, the energy levels at higher frequencies are consequently reduced in the spectrum generated by FitMann, reflected in the lower $\alpha\epsilon^{2/3}$ as compared to the spectrum generated by Mann. The $\alpha\epsilon^{2/3}$ of Mann is found according to Equation 1.

All wind fields are generated with similar domain sizes, covering the entire rotor. The grid size in the rotor plane is 3.5 m, and the time step is about 0.1 s. Six realizations of one hour each are run for TIMESR, Mann and FitMann in order to reduce statistical uncertainty. A previous study [18] found that the IEC recommendation [1] of a total of one hour simulation is insufficient when comparing the responses, in particular in the low-frequency region. The results presented in this study correspond to the mean of the six 1-hour realizations.

We analyse the variations in turbulent structures in the wind fields generated by TIMESR, Mann and FitMann by their spectra and coherence. The turbulence intensities and wind profiles obtained by the different methods are similar to the values given in Table 1. The wind spectra are estimated as outlined above.

The root-coherence is calculated from the cross-spectrum, S_{xy}, and the auto-spectra, S_{xx} and S_{yy}, of two time series separated in space, according to Equation 3.

$$|\gamma| = \frac{|S_{xy}|}{\sqrt{S_{xx}S_{yy}}}. \quad (3)$$

Only the real part of the coherence ($\mathrm{Re}(\gamma)$) of the wind speed in the along wind direction is considered in this study. In other words, the uu-co-coherence is referred to as simply coherence. The imaginary part of the coherence, the quad-coherence ($\mathrm{Im}(\gamma)$), is disregarded. In TIMESR,

the Davenport coherence model is used, according to Equation 4.

$$\gamma = \exp\left(- C * \frac{f\delta}{\overline{u}_m} \right). \tag{4}$$

The Davenport coherence model is dependent on frequency, f, separation distance between the two considered time series, δ, mean wind speed, $\overline{u}_m$, and a decay coefficient, C. In TIMESR, the decay coefficients of the u, v and w components are calculated from the time series of FINO1 separated vertically.

The wind characteristics described by the wind spectra and the coherence influence the response of the wind turbine. The response in the low-frequency region is mainly quasi-static. The shape of the wind spectrum is expected to have strong impact on the response spectra of the blade root and tower bottom bending moments, as discussed in more detail in Nybø et al. [18].

Considering coherence of separation distances of about 0.5-1 rotor diameter, we can expect the following. In a fully coherent wind field, a homogeneous load hits the rotor, causing large bending at the tower bottom. The same is seen for a homogeneous load hitting the blade causing large moments at the blade root. With lower coherence, loads will partly cancel out and therefore cause low bending at the tower bottom, while high local moments at the tower top. Low horizontal coherence is expected to cause high yaw moments, while low vertical coherence is expected to cause high fore-aft moments at the top.

2.2. Response

The aero-hydro-servo-elastic tool, SIMA [26], is used for the wind turbine simulations. The interactions between the wind and the turbine are in this simulation tool computed using the blade element momentum theory. The different wind fields are used as inputs to SIMA, and the various responses are given as outputs.

The analyses are performed on the DTU reference turbine with a bottom-fixed foundation [18]. This wind turbine has a rated power of 10 MW, a rated wind speed of 11.4 m/s, a hub height 119 m and a diameter of 178.3 m [27].

The tower top yaw moment, M_z, the tower top bending moment fore-aft, $M_{T,y}$, the tower bottom bending moment fore-aft, $M_{B,y}$, and the blade root flapwise bending moment, M_F, are considered in this study. Side-side moments are excluded as these are much smaller than the fore-aft moments when subject to only wind loads. No sea waves are present in the simulations. In this study, only the dynamic response of the wind turbine is analysed. Mean values are not assessed.

The response spectra and damage equivalent moments are presented in the following. The response spectra are obtained using the same procedure as for the wind spectra. The damage equivalent moments, referred to as DEM, indicate the wind loads' impact on the structural fatigue. The DEM is calculated according to Equation 5, where R_i is the amplitudes of the response time series, n_i is the corresponding numbers of cycles, and m the Wöhler curve exponent of the material [28]. Rainflow counting is used to isolate and define cycles into individual events. The obtained equivalent moment, R_{eq}, is related to the equivalent number of load cycles in the length of the time series, n_{eq}, assuming a frequency of 1 Hz for the equivalent load process.

$$R_{eq} = \left(\frac{\Sigma_i (R_i^m n_i)}{n_{eq}} \right)^{1/m}. \tag{5}$$

In this study, the value of m is 10 (composite material) for the calculation of the blade equivalent moment and 3 (steel) for the calculation of the tower equivalent moments. It should be kept in mind that the differences across methods obtained in this study would be even larger if one rather compared the fatigue lifetime of the structure.

It is found in a previous study [18] that the low-frequency region (f < 0.1 Hz) has major impact on the total DEM of the wind turbine for the current configuration. The low frequencies were found to be of particular importance for the tower bottom and blade root flapwise bending moment. In the following we thus focus on the low-frequency response. These values are found by low-pass filtering the response time series at 0.1 Hz prior to calculating the DEM.

3. Results and discussion

3.1. Wind fields

The wind fields generated by TIMESR, Mann and FitMann are compared to each other, and to measurements where possible. All wind fields have equivalent turbulence intensity and mean wind speed profile, thus only the turbulent structures are compared.

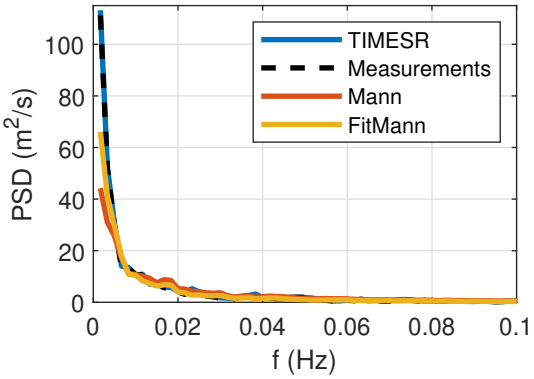

Figure 2. Wind spectra at 80 m for f < 0.1 Hz in *linear* scales. PSD = Power spectral densities. Frequency step, Δf = 0.0017 Hz.

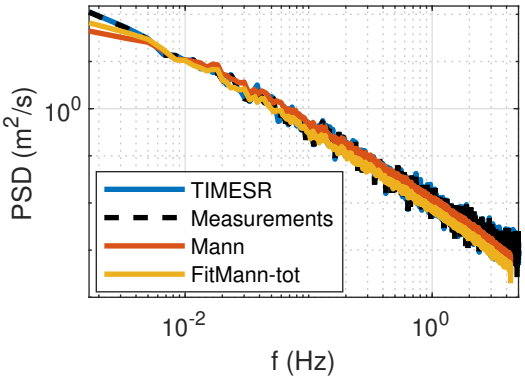

Figure 3. Wind spectra at 80 m in *logarithmic* scales. PSD = Power spectral densities. Frequency step, Δf = 0.0017 Hz.

The wind spectra at 80 m are shown in Figures 2–3. As the spectral values increase as the frequency tends to zero, the results are sensitive to the duration of the time series considered. TIMESR is able to reproduce the spectrum of measurements at 80 m with high accuracy in the complete frequency region. The spectrum generated by the Mann model has lower energy than the measurements in the lowest range of frequencies. The Mann model is made for neutral atmospheric conditions. The chosen situation seems to be closer to slightly unstable atmospheric conditions than slightly stable, with lots of energy in the very low-frequency region, a relatively high TI and a relatively low power law exponent. Compared to the wind spectrum generated by Mann, the wind spectrum generated by FitMann approaches measurements at low frequencies, which are important for response, but falls below at higher frequencies. This is according to expectations considering the input values given in Table 2. The spectra at hub height (not shown), are very similar to those shown in Figures 2–3.

The coherence of vertical separation distances is shown in Figures 4–5. As expected, the coherence of all models is high at low frequencies, corresponding to large eddies, and decays towards zero for higher frequencies and smaller eddies. The decay of coherence is similar across models for small (40 m) and large (125 m) separation distances. TIMESR, Mann and FitMann all model coherence similarly to the measurements (Figure 4), at least for frequencies below 0.05 Hz. The decay parameters of TIMESR are calculated from measurements, but the coherence is assumed to follow a simple model, Davenport. A previous study has shown that the fit to Davenport is good for neutral situations at FINO1 [29]. However, Figure 4 shows that the

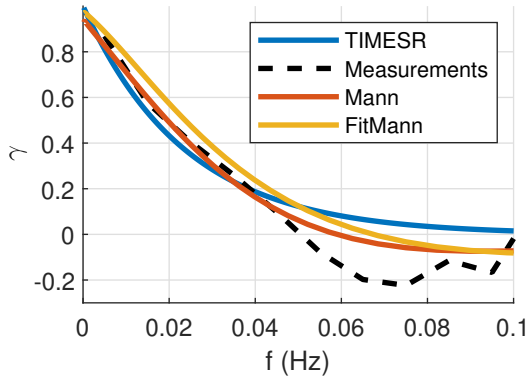

Figure 4. Coherence between two time series separated *vertically* by 40 m (0.22 D). The coherence of measurements is bin-averaged and the coherence of models are based on their respective formulas; thus the smooth curves.

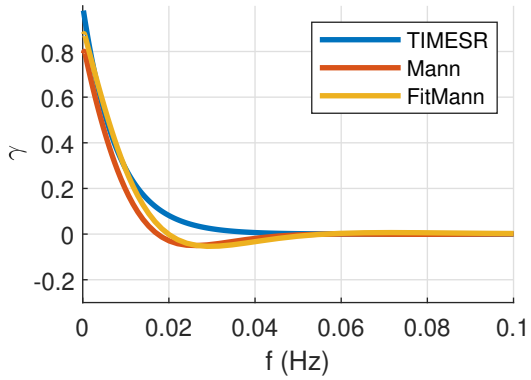

Figure 5. Coherence between two time series separated *vertically* by 125 m (0.7 D). The coherence of models are based on their respective formulas; thus the smooth curves.

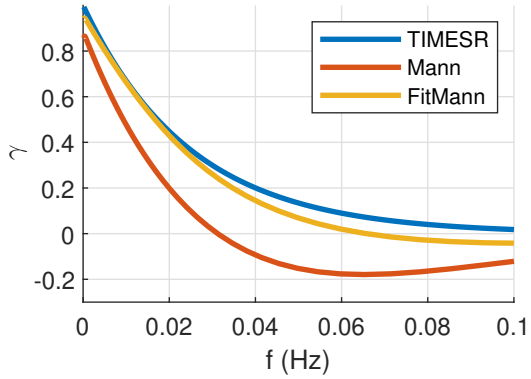

Figure 6. Coherence between two time series separated *horizontally* by 40 m (0.22 D). The coherence of models are based on their respective formulas; thus the smooth curves.

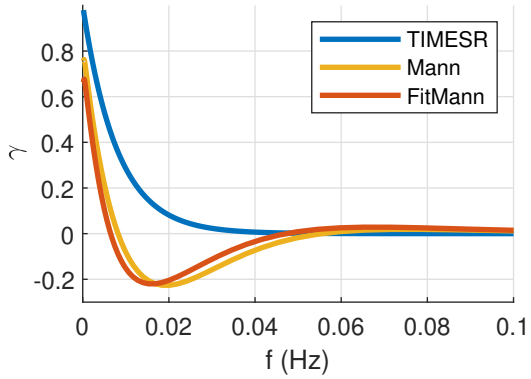

Figure 7. Coherence between two time series separated *horizontally* by 125 m (0.7 D). The coherence of models are based on their respective formulas; thus the smooth curves.

coherence of measurements is negative at some frequencies, which the Davenport model is not able to reproduce.

The Mann model predicts a significant quad-coherence ($\mathrm{Im}(\gamma)$) between two time series separated vertically (not shown), but it is common to disregard this imaginary part of the coherence in the literature [17, 30, 31]. A previous study [18] has shown that the assumption of minor impact of quad-coherence on the response of the current configuration (DTU 10-MW bottom-fixed, for M_z, $M_{T,y}$, $M_{B,y}$ and M_F) is fair.

Figures 6–7 show the coherence between two time series separated horizontally. No measurements are available for this case. TIMESR predicts a slowly decaying coherence, while the coherence generated by Mann decays fast to a bottom at negative values before reaching zero. At large distances (0.7 D = 125 m), the coherence generated by FitMann follows the coherence generated by Mann (Figure 7). The coherence generated by FitMann approaches the coherence

generated by TIMESR for smaller separation distances, ending up in similar coherence curves at 0.22 D = 40 m (Figure 6). Again, it should be kept in mind that TIMESR corresponds to the Davenport coherence model with decay parameters obtained from measurements separated vertically. As no measurements of horizontal coherence are considered in this study, it is not possible to determine which model predicts horizontal coherence most realistically. The value of the horizontal coherence is important for e.g. yaw loads. Thus, altering the input parameters for the Mann model may alter yaw loads, even though no direct fitting of the coherence is performed.

3.2. Response

The wind fields generated by TIMESR, Mann and FitMann are used as input in SIMA, and the corresponding response of the bottom-fixed wind turbine is given as output. In the following, the computed responses as obtained by using the various wind fields are compared. The low-frequency part (f $<$ 0.1 Hz) of the response spectra is used in the comparison. The corresponding DEM allows for comparisons of the fatigue damage of the wind turbine when subject to the different wind fields. The DEM of the low-frequency and complete frequency range are assessed.

The low-frequency response spectra of the tower bottom bending moment fore-aft, $M_{B,y}$, are shown in Figure 8. TIMESR, Mann and FitMann all cause high energy levels at the very first frequencies, followed by a sharp decay. TIMESR causes higher response in $M_{B,y}$ than FitMann, which again causes higher response than Mann. There are great similarities between the wind spectra, Figure 2, and the response spectra, Figure 8, as should be expected due to the combined effect of quasi-static response and a high coherence. As shown in Figures 4–7, TIMESR generates a higher coherence than Mann and FitMann at most frequencies, also pointing towards higher tower bottom response. High coherence causes a large homogeneous force at tower top, and corresponding large moments at the tower bottom. Figures 12–15 show the DEM of the low-pass filtered response time series (f $<$ 0.1 Hz) by squares, and the DEM of the total response time series by circles. The squares of Figure 12 confirm the trends from the response spectra; TIMESR causes the highest damage, followed by FitMann (21 % lower than TIMESR) and Mann (38 % lower than TIMESR). Low frequencies dominate for the total DEM of $M_{B,y}$, clearly shown by the small difference between the low-frequency DEM and the DEM of the total time series. This is in contrast to the other responses considered, Figures 13–15, where there are larger gaps between DEM of low and all frequencies. The differences between models are approximately the same for the low-frequency DEM and the total DEM of $M_{B,y}$ (FitMann 18 % lower than TIMESR and Mann 27 % lower than TIMESR in total DEM). A correct representation of the wind spectrum and the coherence at low frequencies are of utmost importance for a good estimation of the total DEM of $M_{B,y}$.

There are great similarities in the response of the blade root (Figures 9 and 13) and the tower bottom bending moments (Figures 8 and 12). The blade root damage equivalent bending moments of FitMann and Mann are 18 % and 39 % lower than TIMESR when considering only the low frequencies, and 5 % and 12 % when considering the whole frequency range. The shape of the wind spectra has great impact on the response of the blade root flapwise bending moment, M_F. Compared to the tower top, there is much more energy at the very lowest frequencies in the response spectra of $M_{B,y}$ and M_F. As seen from Figure 2, the wind spectrum generated by FitMann is much closer to TIMESR than Mann at the very first frequencies, but it still has significantly lower energy levels. As previously mentioned, the large energy levels at low frequencies (and the low power law exponent) of the chosen situation indicate that the near-neutral atmospheric conditions are closer to unstable than stable. If a situation with atmospheric conditions closer to neutral were chosen, the gap between TIMESR and Mann/FitMann in the energy spectrum could possibly be reduced. Consequently, a smaller gap between TIMESR and Mann/FitMann in the response of $M_{B,y}$ and M_F would be expected. In order to improve

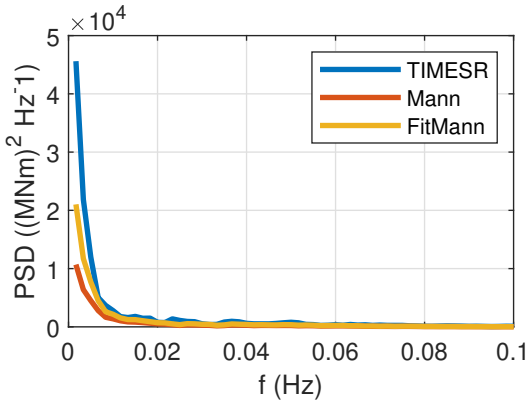

Figure 8. $M_{B,y}$ response spectra of the wind turbine subject to various input wind fields. PSD = Power spectral densities. Frequency step, Δf = 0.0017 Hz.

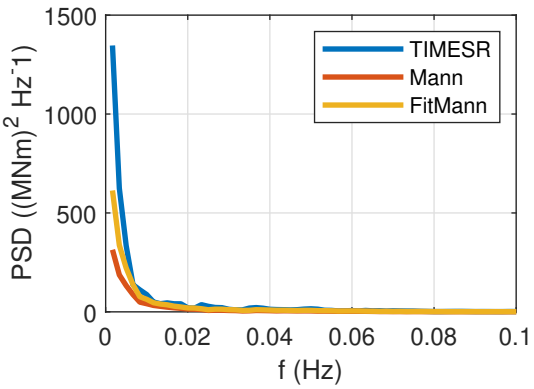

Figure 9. M_F response spectra of the wind turbine subject to various input wind fields. PSD = Power spectral densities. Frequency step, Δ = 0.0017 Hz.

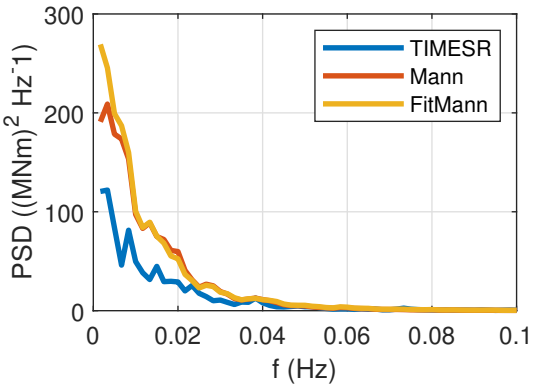

Figure 10. M_z response spectra of the wind turbine subject to various input wind fields. PSD = Power spectral densities. Frequency step, Δf = 0.0017 Hz.

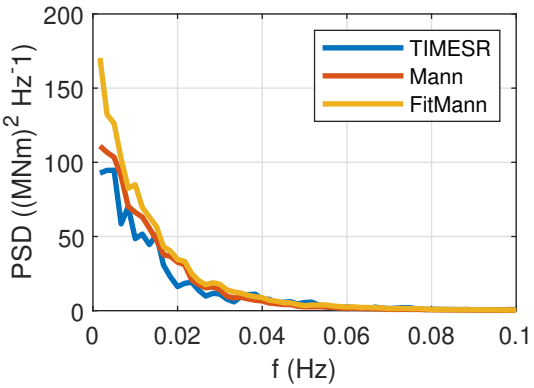

Figure 11. $M_{T,Y}$ response spectra of the wind turbine subject to various input wind fields. PSD = Power spectral densities. Frequency step, Δf = 0.0017 Hz.

the fit of the wind spectrum at very low frequencies, we found alternative FitMann-parameters by fitting the Mann spectrum to only the low-frequency region (f < 0.1 Hz) of measurements. The wind spectrum of the alternative fit is slightly higher at the very lowest frequencies, at the expense of a poorer fit and lower energy levels already at 0.0067 Hz and upwards. The response of $M_{B,y}$ and M_F when using the wind field generated by TIMESR as input is assumed to be quite realistic as the wind spectrum of measurements is reproduced in the model, and the shape of the wind spectrum has great impact on these responses. The DEM of the total response time series of the alternative Mann fitting is further away from TIMESR than the original FitMann at both $M_{B,y}$ and M_F, thus the alternative Mann fitting is disregarded from further analysis.

Focusing on the tower top yaw moment, M_z, one observes a slower decay of the response spectra towards higher frequencies compared to the tower bottom and blade root (Figure 10). There are large differences between the response of using wind fields generated by TIMESR and the two Mann models, but minor differences between using wind fields generated by Mann and FitMann as input in the wind turbine response analysis. The response of using wind

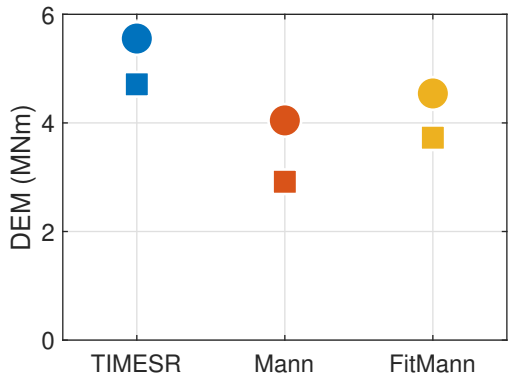

Figure 12. $M_{B,y}$ damage equivalent moments of the wind turbine subject to various input wind fields. □ = DEM of low frequencies (f < 0.1 Hz), ○ = DEM of all frequencies.

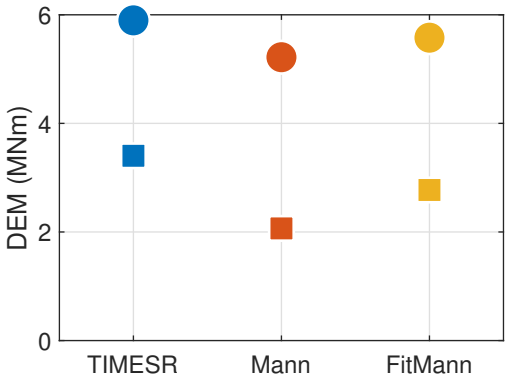

Figure 13. M_F damage equivalent moments of the wind turbine subject to various input wind fields. □ = DEM of low frequencies (f < 0.1 Hz), ○ = DEM of all frequencies.

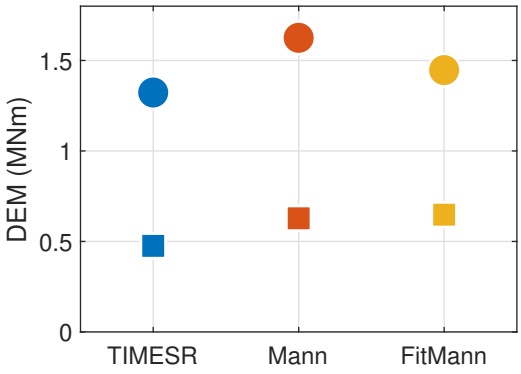

Figure 14. M_z damage equivalent moments of the wind turbine subject to various input wind fields. □ = DEM of low frequencies (f < 0.1 Hz), ○ = DEM of all frequencies.

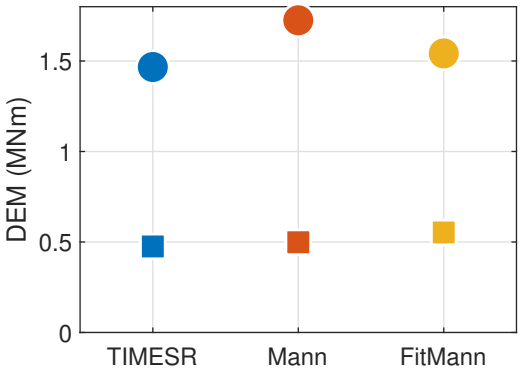

Figure 15. $M_{T,Y}$ damage equivalent moments of the wind turbine subject to various input wind fields. □ = DEM of low frequencies (f < 0.1 Hz), ○ = DEM of all frequencies.

fields generated by Mann or FitMann is higher compared to using the wind field generated by TIMESR for M_z. The yaw response is strongly impacted by the wind spectra and the horizontal coherence. Uncorrelated eddies in the horizontal direction (low coherence) cause local loads and corresponding yaw moments. Figure 7 shows that the coherence generated by Mann and FitMann is much lower than that of TIMESR at 0.7 D, and even negative at some frequencies. The coherence generated by Mann stays significantly lower than that of TIMESR for all relevant separation distances, while the coherence generated by FitMann approaches that of TIMESR towards 0.2 D. The high response of using wind fields generated by Mann and FitMann is reflected in the DEM of the low-frequency range, see Figure 14. The DEM of the low-frequency range of Mann and FitMann are 32 % and 36 % higher than TIMESR respectively. Low frequencies have less impact on the total DEM at tower top than tower bottom. This is observed by the relatively large distance between the DEM of the low frequencies and the

DEM of the complete frequency range. Considering the DEM of the complete frequency range, using the wind field generated by FitMann causes a response similar to using the wind field generated by TIMESR (FitMann 9 % higher than TIMESR), as compared to using the wind field generated by Mann (Mann 23 % higher than TIMESR). It is still not reasonable to conclude that FitMann causes a more realistic response than Mann. The yaw response is as mentioned strongly influenced by the horizontal coherence. As this study includes no measurements of the horizontal coherence, it is impossible to determine which model estimates the horizontal coherence most realistically. The resulting DEM of all frequencies of using the wind field generated by FitMann is closer to the resulting DEM of using the wind field generated by TIMESR as compared to using the wind field generated by Mann, probably because of the lower energy levels at frequencies higher than 0.1 Hz in the wind spectrum. The rotation frequencies (3P, 6P, 9P etc.) have larger impact on the response at tower top than at tower bottom. The higher coherence generated by FitMann at smaller separation distances may also have an impact on the response at higher frequencies.

There are great similarities in the response of the tower top bending moment fore-aft (Figures 11 and 15) and the tower top yaw moment (Figures 10 and 14). Low coherence is expected to cause high response of both. The tower top bending moment fore-aft, $M_{T,y}$, is stronger influenced by the vertical coherence, which is quite similar across methods. This is reflected in the response, where there are slightly less differences in the fore-aft response than yaw. The $M_{T,y}$ DEM of FitMann and Mann are 16 % and 5 % higher than TIMESR when considering only the low frequencies, and 5 % and 18 % when considering the whole frequency range. Following the same logic as for the tower top yaw, uncorrelated eddies in the vertical direction (less vertical coherence) cause local loads and corresponding fore-aft moments at the tower top.

4. Conclusions and further work

In this study, we have modelled offshore wind fields using various techniques and by fitting parameters using measured wind data. The wind field generated by TIMESR is closely based on measurements, the wind field generated by Mann is made with only TI fitted to site, while the wind field generated by FitMann is based on the same model as Mann, but with input parameters fitted to the wind spectra of measurements. The three models are compared in terms of spatial and temporal distribution of turbulent structures, before they are used as input in wind turbine simulations. As expected, the wind spectrum generated by TIMESR reflects the measurements better than the wind spectrum generated by Mann with standard parameters. The Mann model does not reach the high energy levels of measurements at low frequencies. The wind spectrum generated by FitMann approaches the wind spectrum generated by TIMESR at low frequencies, important for response, while it falls below at very high frequencies. The findings are based on wind fields fitted to one hour of measurements. The trends of the results are still expected to be valid for most situations. FitMann will represent the wind spectrum of measurements better than Mann, due to the fitting of the input parameters. However, the quantitative differences across models will vary depending on the chosen situation. Considering coherent structures, the three models predict similar coherence between two time series separated vertically, while FitMann and especially Mann predict much lower coherence than TIMESR for time series separated horizontally.

It is clear that the low-frequency region of the wind spectra has major impact on the response of the tower bottom and blade root bending moments. TIMESR, using input time series to model wind spectra, is therefore assumed to cause the most realistic response at tower bottom and blade root. The smaller gap between the wind spectra generated by FitMann and TIMESR than Mann and TIMESR at low frequencies is reflected in the response spectra. Therefore, we conclude that using a wind field generated by FitMann as input in wind turbine design analysis

when evaluating the response of the tower bottom bending moment fore-aft and blade root flapwise bending moment of a bottom-fixed wind turbine most likely gives more realistic results than using the Mann formulation with standard parameters. Again, the quantitative differences across models will vary depending on the chosen period of measurements.

The results show that the response at low frequencies ($f < 0.1$ Hz) has major impact on the total damage equivalent moments of the tower bottom bending fore-aft. It is therefore important to model the wind spectra and coherence of these frequencies correctly in order to achieve a correct representation of the fatigue damage at tower bottom.

The measurements from the offshore mast provide no information on the coherence of time series separated horizontally, and only limited information on the coherence of time series separated vertically. Therefore, we are not able to conclude which model predicts coherence most realistically. The coherence has large impact on the response at tower top. We are not able to conclude whether using the wind field generated by FitMann as input in wind turbine design analysis when evaluating the response of the tower top yaw moment and the tower top bending moment fore-aft cause more realistic results than using the wind fields generated by TIMESR or Mann.

This study has shown that there are significant differences in response across models even when a neutral atmospheric stability situation is considered. It is expected that Mann with standard inputs is more capable of representing neutral than non-neutral situations. If fit to other stability conditions, we expect to see larger differences between models, so FitMann may improve the results even further. Further work should include a fit to unstable and stable situations in the analysis.

Acknowledgments
The authors would like to thank Etienne Cheynet, a colleague at Bergen Offshore Wind centre and Geophysical Institute, for his support on fitting of Mann parameters and corresponding analysis.

References

[1] International Electrotechnical Commission 2019 *IEC 61400-1 Wind energy generation systems - Part 1: Design requirements* (Geneva)
[2] International Electrotechnical Commission 2019 *IEC 61400-3-1 Wind energy generation systems - Part 3-1: Design requirements for fixed offshore wind turbines* (Geneva)
[3] International Electrotechnical Commission 2019 *IEC TS 61400-3-2 Wind energy generation systems - Part 3-2: Design requirements for floating offshore wind turbines* (Geneva)
[4] Mann J 1994 *J. Fluid. Mech.* **273** 141–68
[5] Mann J 1998 *Probabilist. Eng. Mech.* **13** 269–82
[6] Sathe A, Mann J, Barlas T, Bierbooms W A A M and van Bussel G J W 2013 *Wind Energy* **16** 1013–32
[7] De Maré M and Mann J 2014 *J. Phys.: Conf. Ser.* **524** 012106
[8] Cheynet E 2019 Influence of the measurement height on the vertical coherence of natural wind *Proc. of the XV Conf. of the Italian Association for Wind Engineering (Napoli)* vol 27 ed Ricciardelli F and Avossa A M (Cham: Springer) pp 207–21
[9] Cheynet E, Jakobsen J B and Obhrai C 2017 *Enrgy. Proced.* **137** 414–27
[10] Peña A, Gryning S E, Mann J and Hasager C B 2010 *J. Appl. Meteorol. Clim.* **49** 792–806
[11] Peña A, Gryning S E and Mann J 2010 *Q. J. Roy. Meteor. Soc.* **136** 2119–31
[12] Chougule A, Mann J, Segalini A and Dellwik E 2015 *Wind Energy* **18** 469–81
[13] Chougule A, Mann J, Kelly M and Larsen G C 2017 *J. Atmos. Sci.* **74** 949–74
[14] Chougule A, Mann J, Kelly M and Larsen G C 2018 *Bound.-Lay. Meteorol.* **167** 371–97
[15] Ghobadi M 2016 DNV GL brings wind industry leaders together in "Validation of Turbulence Models" - DNV GL URL `https://www.dnvgl.com/news/dnv-gl-brings-wind-industry-leaders-together-in-validation-of-turbulence-models--77607`
[16] Jonkman B J 2016 *TurbSim User's Guide v2.00.00* (Golden)
[17] Veers P S 1988 *Three-Dimensional Wind Simulation* (Albuquerque: Sandia National Labs)
[18] Nybø A, Nielsen F G and Godvik M 2021 *Wind Energ.* 1–19
[19] Nybø A, Nielsen F G and Reuder J 2019 *J. Phys. Conf. Ser* **1356** 012006

[20] Türk M, Grigutsch K and Emeis S 2008 *DEWI-Magazin*
[21] DTU Wind Energy 2018 Pre-processing tools URL `http://www.hawc2.dk/download/pre-processing-tools`
[22] Davenport A G 1961 *Q. J. Roy. Meteor. Soc.* **87** 194–211
[23] Cheynet E 2020 ECheynet/fitMann1994 1.3 URL `https://zenodo.org/record/3774088`
[24] Welch P D 1967 *IEEE Trans. Audio Electroacoust.* **15** 70–3
[25] Cheynet E 2020 ECheynet/binAveraging: Averaging noisy data into bins URL `https://zenodo.org/record/3818011`
[26] Hermundstad O A Sima - SINTEF URL `https://www.sintef.no/programvare/sima/`
[27] Bak C, Zahle F, Bitsche R, Yde A, Henriksen L C, Nata A and Hansen M H 2013 *Description of the DTU 10 MW Reference Wind Turbine*
[28] International Electrotechnical Commision 2015 *IEC TS 61400-13: Wind turbine generator systems - Part 13: Measurement of mechanical loads* (Geneva)
[29] Cheynet E, Jakobsen J B and Reuder J 2018 *Bound.-Lay. Meteorol.* **169** 429–60
[30] Eliassen L and Obhrai C 2016 *Enrgy. Proced.* **94** 388–98
[31] Saranyasoontorn K, Manuel L and Veers P S 2004 *J. Sol. Energ-T. Asme* **126** 1069–82